LETTERS
PUBLISHED ONLINE: 30 MAY 2010 | DOI: 10.1038/NNANO.2010.86
nature nanotechnology

Spontaneous high-concentration dispersions and liquid crystals of graphene

Natnael Behabtu[1,3‡], Jay R. Lomeda[2,3‡], Micah J. Green[1,3†], Amanda L. Higginbotham[2,3], Alexander Sinitskii[2,3], Dmitry V. Kosynkin[2,3], Dmitri Tsentalovich[1,3], A. Nicholas G. Parra-Vasquez[1,3], Judith Schmidt[4], Ellina Kesselman[4], Yachin Cohen[4], Yeshayahu Talmon[4], James M. Tour[2,3,5*] and Matteo Pasquali[1,2,3*]

Graphene combines unique electronic properties and surprising quantum effects with outstanding thermal and mechanical properties[1–4]. Many potential applications, including electronics and nanocomposites, require that graphene be dispersed and processed in a fluid phase[5]. Here, we show that graphite spontaneously exfoliates into single-layer graphene in chlorosulphonic acid, and dissolves at isotropic concentrations as high as ~2 mg ml^{-1}, which is an order of magnitude higher than previously reported values. This occurs without the need for covalent functionalization, surfactant stabilization, or sonication, which can compromise the properties of graphene[6] or reduce flake size. We also report spontaneous formation of liquid-crystalline phases at high concentrations (~20–30 mg ml^{-1}). Transparent, conducting films are produced from these dispersions at 1,000Ω □$^{-1}$ and ~80% transparency. High-concentration solutions, both isotropic and liquid crystalline, could be particularly useful for making flexible electronics as well as multifunctional fibres.

Many promising macroscopic applications of graphene require the development of new routes for effective graphite exfoliation and processing[1,7]. Micromechanical cleavage[8], the first reported method to isolate graphene from graphite, has extremely low yield and cannot be used in bulk applications. Large amounts of graphene sheets can be obtained by oxidizing graphite layers through various processes to yield water-soluble graphene oxide[9,10]. Further chemical reduction and derivatization yield functionalized graphene that is soluble in common organic solvents[5]. Although functional groups aid dissolution, they also compromise many of graphene's desirable electrical and thermal properties[6]. Reduction of graphite oxide only partially restores these properties[11]. Liquid phase dispersion in organic solvents—for example, *N*-methyl pyrrolidone (NMP)—can be attained without chemical modification by sonication[12] or by potassium intercalation without sonication[13]. Graphene has also been dispersed in water by sonication and stabilization using surfactants[14]. However, liquid-phase dispersions yield low concentrations (0.01 mg ml^{-1}, ref. 12; 0.15 mg ml^{-1}, ref. 13), and sonication limits the size of graphene flakes achievable.

Superacids have been successfully used to dissolve single-walled carbon nanotubes (SWNTs) and show great promise for the bulk processing of SWNT-based materials[15]. Chlorosulphonic acid, the most promising SWNT solvent, was first produced in 1854 and today is a commodity chemical with a production of more than 300,000 tons per year. It is used chiefly as a sulphonating chemical in detergent and dye production[16]. Although the intercalation of graphite by strong acids, including chlorosulphonic acid, has been studied for decades[17], there are no reports indicating that graphite is soluble in strong acids.

In this study the behaviour of pristine graphite in chlorosulphonic acid was investigated. Three different sources of graphite were used: graphoil (commercial graphitic material used in seals), microcrystalline graphite and highly ordered pyrolytic graphite (HOPG). The concentration of the dispersed phase was determined by centrifuging the initial dispersion, extracting the top (isotropic) phase, and measuring its absorbance by UV–vis–NIR (near-infrared) spectra. Figure 1a shows that the acid disperses graphene from various graphite sources at high concentrations without sonication; these isotropic solutions are ten to a hundred times more concentrated than those previously attained by sonicating graphite in organic solvents or in water in the presence of surfactants. The UV–vis–NIR spectrum is featureless as a function of wavenumber (Supplementary Fig. S1a), in agreement with previous reports[12]. The phase separation that occurs during centrifugation is not an equilibrium one; instead, a fraction of the original material goes into solution while the remainder is insoluble (Supplementary Fig. S2). This is similar to observations for surfactant and NMP dispersions[12,14].

Acid strength affects dispersion quality. We controlled acid strength by mixing chlorosulphonic acid and concentrated (98%) sulphuric acid in varying proportions[18] (hereafter, mixed solvents are denoted by the concentration of chlorosulphonic acid). The insert in Fig. 1b shows that graphite solubility decreased markedly as the acidity was lowered to 80% chlorosulphonic acid, and solubility dropped further as acidity was lowered. For comparison, we dispersed the same material in NMP, an organic solvent previously reported for pristine graphene dissolution. Without sonication, the level of dispersion in NMP was negligible.

We next investigated the mechanism of graphene dissolution in superacids. Earlier work with superacid/SWNT solutions showed that dispersion is due to protonation of the SWNT sidewalls, which causes electrostatic repulsion and debundling. The degree of protonation (positive charge per carbon atom) in graphitic materials is measured through the acid-induced shift (dG) in the location of the G peak in the Raman spectra[18–20]. Figure 1b reports dG for the various acid mixtures; the Raman shift dG

[1]Department of Chemical and Biomolecular Engineering, Rice University, Houston, Texas 77005, USA, [2]Richard E. Smalley Institute for Nanoscale Science and Technology, Rice University, Houston, Texas 77005, USA, [3]Department of Chemistry, Rice University, Houston, Texas 77005, USA, [4]Department of Chemical Engineering, Technion—Israel Institute of Technology, Haifa 32000, Israel, [5]Department of Mechanical Engineering and Materials Science, Rice University, Houston, Texas 77005, USA; [†]Present address: Department of Chemical Engineering, Texas Tech University, Lubbock, Texas 79409, USA; [‡]These authors contributed equally to this work. *e-mail: tour@rice.edu; mp@rice.edu

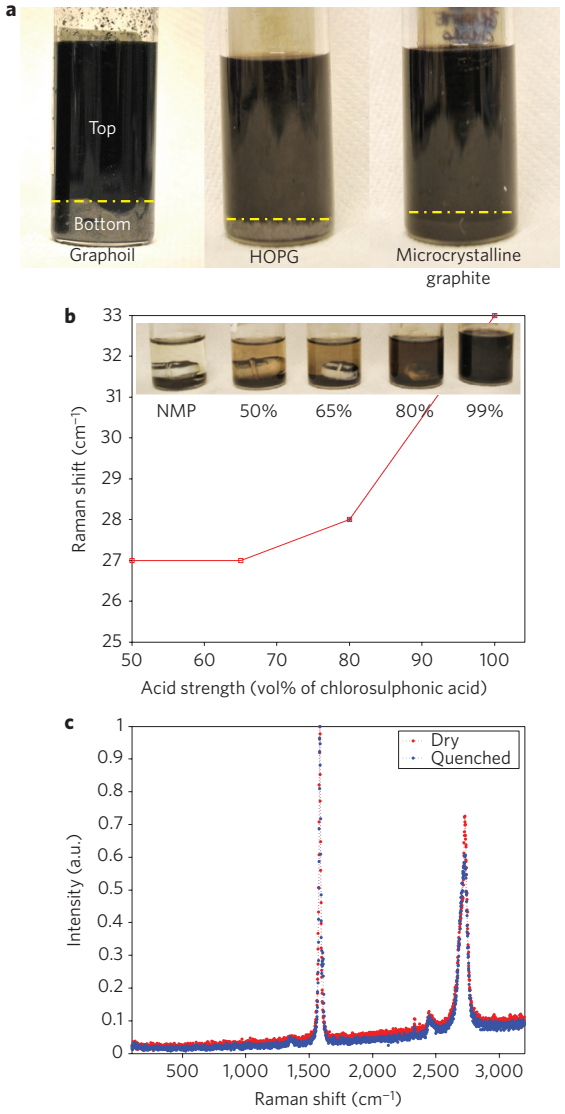

Figure 1 | Solubility and solvent quality of graphite dispersions. **a**, Comparison of chlorosulphonic acid dispersion of graphite (25 mg ml^{-1} initial concentration) obtained from different sources as indicated below the vials. A dark upper portion (top) is obtained for all the sources after 12 h of centrifugation (5,000 r.p.m.), with a grey-coloured lower portion (bottom). The yellow line on the vials indicate the interface between the top and bottom phases in the three vials. The soluble portion was removed and isolated for solubility determinations. **b**, Comparison of acid-induced shifts in the liquid-phase Raman G-peak for graphite dispersed in the same mixtures of chlorosulphonic acid in sulphuric acid. The G-peak shift, denoted as dG, is a quantitative measure of the degree of protonation. The image in the insert shows a qualitative comparison between graphite dissolution into different solvents, showing graphite in the vials with a Teflon-coated stir bar to promote dissolution. Starting from the left, graphite is dissolved in NMP, 50, 65 and 80 vol% chlorosulphonic acid (HSO_3Cl) in sulphuric acid (H_2SO_4) and pure chlorosulphonic acid. The dispersions were prepared at 10 mg ml^{-1}. The acid dispersions were then centrifuged at 5,000 r.p.m. for 12 h and the NMP dispersion was centrifuged for 3 h. The amount of centrifugation time is different for the two cases because the settling time is linearly dependent on the density differential between the particles and solvent. Thus, the centrifugation time is scaled by this density difference. **c**, Solid-state Raman spectra of the initial graphite dry powder and the graphite quenched from the acid dispersion. The two spectra are virtually identical, indicating that protonation is reversible. Both the liquid- and solid-phase Raman spectra were taken with excitation wavelengths of 514 nm and long working distances on a ×50 lens.

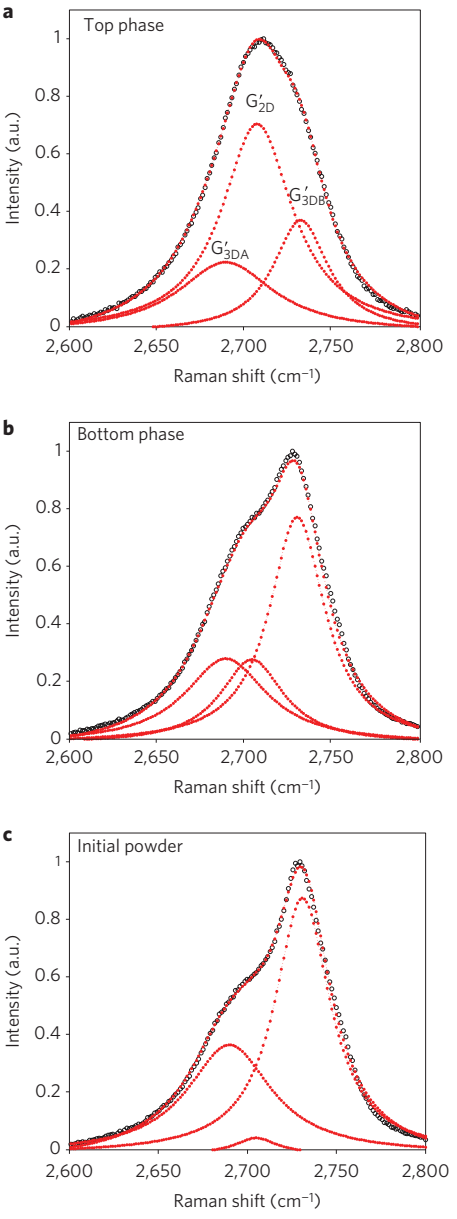

Figure 2 | G′ band Raman spectra performed using an excitation laser wavelength of 514 nm. a–c, Spectra obtained using graphoil as a starting material. The top (**a**) and bottom (**b**) phase spectra were obtained on solid samples by quenching the acid-dispersed material. The experimental curves were fitted with three Lorentzians centred at ~2,690 (G'_{3DA}), 2,710 (G'_{2D}) and 2,730 (G'_{3DA}), respectively. The G′ peak of the top phase is mostly composed of the G'_{2D} peak, and the undispersed bottom phase is mostly composed of G'_{3DA} and G'_{3DB} peaks, although it has a higher G'_{2D} peak compared to the initial graphite powder (**c**).

drops with decreasing acidity, mirroring the decrease in solubility. Figure 1c shows the Raman spectra of a sample of graphite powder before and after acid dissolution, quenching in water and drying. The spectrum is essentially unchanged (in particular, the D-band, characteristic of sp^3 carbon content, remains low, see also Supplementary Fig. S14), so acid dissolution does not introduce defects in the starting material. This indicates no damage or functionalization by the acid, the same behaviour as seen in SWNTs[15]. X-ray photoelectron spectroscopy (XPS) further supports this conclusion (Supplementary Figs S4,S13). Compared to SWNTs, graphene is less soluble in the same acid; SWNTs are soluble in weaker superacids, such as 102% sulphuric acid.

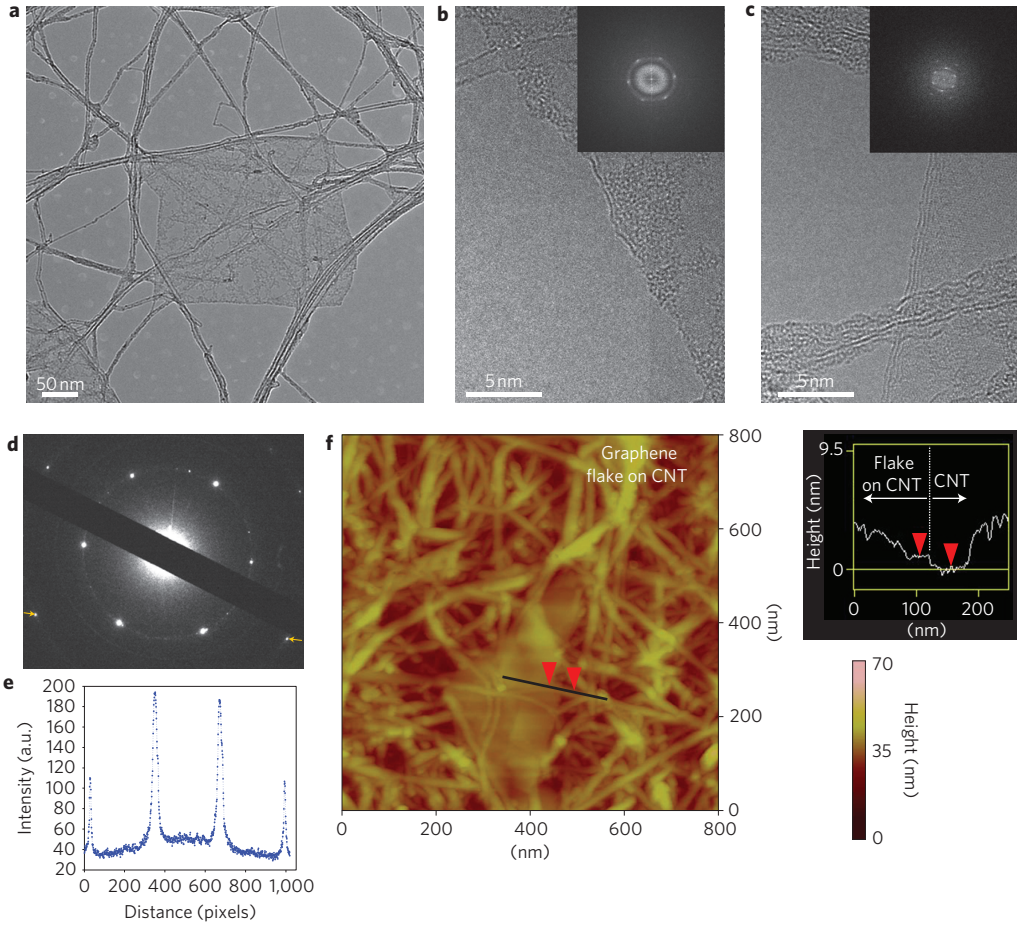

Figure 3 | Evidence for single-layer dissolution. a, Low-magnification TEM showing a small flake of graphene. Note how the CNT network beneath the graphene flake is clearly visible. **b**, HRTEM of a single-layer edge with fast Fourier transform (FFT) insert. **c**, HRTEM of a few-layer edge with its FFT. Adsorbates of unknown origin are clearly visible at high magnification, similar to flakes obtained by micromechanical cleavage[22]. **d**, Electron diffraction showing the typical intensity profile along the line delimited by the two yellow arrows (**e**) (see also the diffraction intensity as a function of tilting angle in S-07). **f**, AFM image and its height profile showing a flake with a height of 0.5 nm.

We further characterized the top and bottom phases to better understand the dispersion mechanism. Raman spectroscopy (Supplementary Fig. S3) shows a higher D-peak in the top than in the bottom phase; this D-peak grows with longer centrifugation time. However, XPS (Supplementary Fig. S4) does not reveal any oxygen or sulphur in the quenched top phase. Therefore, we conclude that the graphite flakes in the top phase are smaller, that is, they have a larger perimeter-to-surface ratio.

We measured the Raman G′ peak, a measure of graphite stacking[21], of the quenched top and bottom portions of the centrifuged sample (Fig. 2). The data show that the quenched top phase loses the typical Bernal stacking of the initial powder and attains the turbostratic stacking typical of disordered graphite, whereas the bottom phase retains most of the Bernal signature of the initial powder.

Conclusive proof of single-layer exfoliation requires transmission electron microscopy (TEM) or atomic force microscopy (AFM). However, the properties of chlorosulphonic acid pose challenges to the preparation of TEM samples (because holey carbon grids dissolve in the acid) and AFM substrates (because the low volatility, high surface tension and hygroscopicity of acid cause substantial re-aggregation). We solved this problem by capturing graphene flakes on custom-made SWNT grids (see Methods) that were then transferred onto a standard grid for TEM or silica substrate for AFM. High-resolution TEM (HRTEM) was then used to image the graphene layers. Figure 3a,b presents low- and high-magnification images of a single-layered graphene flake, and Fig. 3c shows an HRTEM image of a few-layered graphite flake. The SWNT network is clearly visible through the flake. Electron diffraction (Fig. 3d) shows the typical[22] Bragg reflections intensity ratio of single-layer graphene (Fig. 3e). Height determination by AFM was more problematic, because the SWNT network yields a rough background surface (Fig. 3f). However, the height profile of one flake

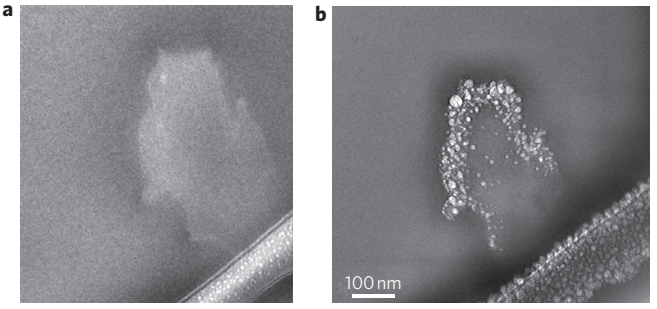

Figure 4 | Graphene as a rigid platelet. a,b, Cryogenic-TEM images of graphene flakes dispersed in chlorosulphonic acid. A graphene flake (**a**) is shown close to the TEM lacey carbon edge at very low imaging conditions (<10 electrons $Å^{-2}$). After some irradiation from the electron beam of 50–80 electrons $Å^{-2}$ (**b**), the contrast between the graphene and acid is heightened close to the graphene edges as acid is preferentially etched at these sites. No dark lines (which indicate folding points) can be observed.

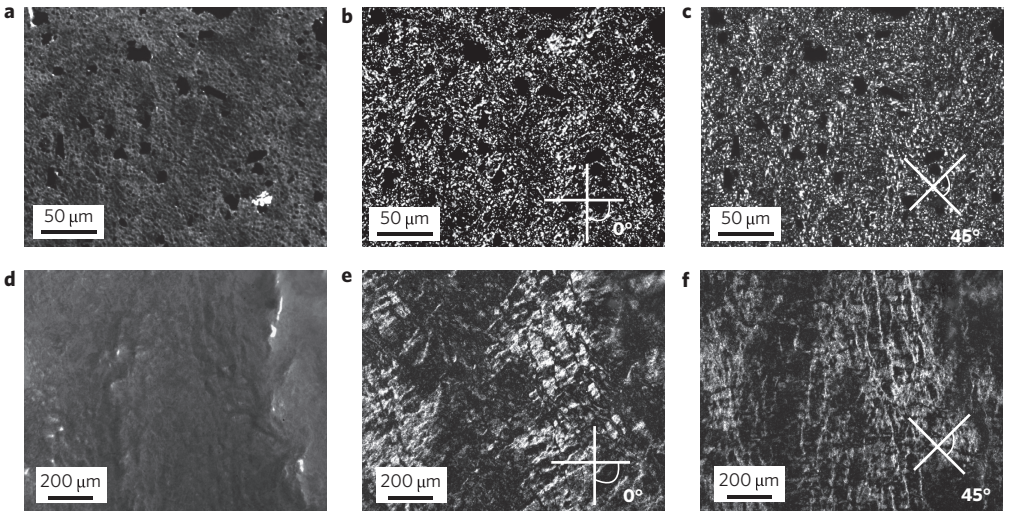

Figure 5 | Evidence for the graphene liquid-crystalline phase. a–c, Light micrographs of a high-concentration (~2 wt%) graphene dispersion in chlorosulphonic acid (scale bar, 50 μm): transmitted light (**a**); transmitted polarized light with analyser and polarizer crossed at 90° (**b**); crossed analyser and polarizer rotated by 45° with respect to image **b** (**c**). **d–f**, Light micrographs of high-concentration (~2 wt%) oxidized nanoribbons dispersion in chlorosulphonic acid (scale bar, 200 μm): transmitted light (**d**); transmitted polarized light with analyser and polarizer crossed at 90° (**e**); crossed analyser and polarizer rotated by 45° with respect to image **e** (**f**).

shows a step height of 0.5 nm, consistent with single-layer graphene. HRTEM and electron diffraction were also used to analyse over 30 flakes and quantify the degree of exfoliation. It was found that 70% of the dispersed graphene flakes were single layer. A combination of scanning electron microscopy (SEM) and scanning transmission electron microscopy (STEM) was used to assess size distribution. We found that the average size depends on graphite source. Microcrystalline graphite and graphoil have an average flake size of 300 and 900 nm, respectively (Supplementary Fig. S9).

Graphene flakes should act roughly as rigid platelets (on the scale of thermal forces) and therefore should be approximately flat in good solvents (S-03). However, intramolecular self attraction or repulsion could alter graphene conformation in solution. The protonation induced by chlorosulphonic acid should induce self repulsion and decrease the likelihood of folding. We imaged graphene flakes under cryo-TEM (Fig. 4a,b) to determine their conformation in solution and found that the flakes are extended. SEM and STEM of graphene flakes captured on SWNT grids from acid solutions further support this conclusion (Supplementary Fig. S6). Rigid anisotropic molecules undergo an isotropic/liquid-crystalline transition as their concentration is raised[23]. Lekkerkerker, Frenkel and colleagues experimentally observed this transition with clay particles and used Onsager-like theories to determine the phase diagram[24,25]. The transition concentration scales inversely with the aspect ratio (diameter/thickness). As in rigid rods[26,27], polydispersity broadens the biphasic region, and both the maximum isotropic concentration of the platelets and the ability to form liquid crystals depends on solvent quality[28].

We tested these concepts in the graphene/superacid systems. The top phase was extracted and quenched after centrifugation. The powder was then redispersed at ~20 mg ml^{-1} and centrifuged to induce phase separation. The top phase is structureless and has a concentration of 1.8 mg ml^{-1}. Under a cross-polarizer, the bottom phase shows birefringence typical of a liquid crystal (Fig. 5a–c). Therefore, unlike the starting material, dispersion of an entirely soluble graphene source yields isotropic/liquid-crystalline phase separation as expected in a solution of rigid platelets. Various liquid-crystalline phases (nematic, chiral, columnar) have been reported for disc-like platelets (called discotics); the nematic phase is the only probable phase for polydisperse, unfunctionalized systems such as ours. The liquid-crystalline Schlieren texture in Fig. 5b,c is very similar to typical discotic nematic samples[29]. This liquid-crystalline phase is promising for processing of neat graphitic macroscopic articles such as fibres and films, particularly in light of recent improvements in graphene size control and bulk manufacturing, such as the production of controlled-size graphene nanoribbons (GNRs)[30–32]. We measured the solubility of both oxidized and reduced GNRs in chlorosulphonic acid as 3.4 mg ml^{-1}. No undispersed material was observed; instead, the entire sample is soluble and forms liquid crystals at high concentration (Fig. 5d–f). Again, the fact that the reduced GNRs are entirely soluble with no precipitate indicates that chlorosulphonic acid disperses graphene at the single-layer level.

High-concentration isotropic solutions are attractive both for nanocomposites and for functionalization of graphene. We used isotropic dispersions to make thin films by filtration, including transparent and conducting films (S-04). One thin film (8 μm thick) was non-transparent but showed a conductivity of 110,000 S m^{-1}; this is comparable to the best graphene film conductivity reported in the literature by solution processing[11]. However, both the ability to form thin free-standing films and the electrical properties are highly dependent on the starting graphite; graphoil yields better films on both measured compared with microcrystalline graphite. The most relevant difference between these two graphite sources is the average graphene flake size in solution. Twelve electronic devices based on thin (~10 nm thick) films exhibited similar conductivity values in the range 80,000–95,000 S m^{-1}. We also measured a sheet resistance of 1,000Ω □$^{-1}$ on an 80% transparent (at 550 nm) film. These values are an order of magnitude better than other films produced from pristine graphene dispersions[12,14] (Supplementary Figs S10–S12).

We have shown that chlorosulphonic acid exfoliates graphite into isotropic graphene dispersions at concentrations one order of magnitude higher than any other known solvent or dispersant. The acid protonates the graphene to induce repulsion between layers; the mechanism is similar to acid protonation of SWNTs and does not damage or functionalize the material[20]. A minimum degree of protonation is required for dissolution at high concentrations. Moreover, chlorosulphonic acid disperses new forms of graphene such as graphene nanoribbons. High-concentration dispersions of fully soluble material yield liquid-crystalline phases. The highly

concentrated isotropic and liquid-crystalline phases are promising for functionalization, and for scalable manufacturing of nanocomposites, films, coatings and high-performance fibres. In particular, we envision graphene liquid crystals as a replacement for traditional discotic pitch-based liquid crystals used as precursors for carbon fibres, films and weaves.

Materials and Methods

We analysed and characterized three different sources of graphite in this study: (i) graphoil (expanded graphite; EGS Enterprises), (ii) microcrystalline graphite (Sigma Aldrich, batch no. 08017EH), and (iii) highly ordered pyrolytic graphite (HOPG) (SPI Supplies, lot no. 1091028). Chlorosulphonic acid (Sigma Aldrich, 99%, batch no. 16096EJ) and sulphuric acid (Fisher Chemical, certified ACS plus, lot no. 083290) were used as solvents.

Raman spectroscopy was performed on a Renishaw Raman microscope using a 514 nm He−Ne laser. Raman spectra of solid samples were taken by depositing the graphite on a glass slide with the aid of double tape. To measure the solid-state Raman spectra of the top and bottom phase of a centrifuged sample, the sample was quenched by the addition of excess water. (Note that extreme care has to be taken during this operation due to the highly exothermic reaction of chlorosulphonic acid with water; dropwise addition of water into the acid is advised. The researcher also needs the appropriate protective equipment.) Once the graphite precipitated, the mixture was filtered to yield a solid sample. To measure the Raman shift in the fluid, samples were prepared in a glovebox (dew point −50 °C, to avoid contact with moisture), deposited on glass slides, covered with cover slips and sealed with wax or tape to prevent moisture ingress during the measurement outside the glovebox. The same procedure was followed for the preparation of microscopy slides.

TEM and HRTEM imaging and electron diffraction were performed using a JEOL 2010 operated at 100 kV and a FEI Titan 80-300 S/TEM operated at 300 kV with a point-to-point resolution below 1 Å.

The cryo-TEM techniques followed those of Davis and colleagues[15]. The standard cryo-TEM procedure[33] was modified to account for unique difficulties associated with working with superacids. Soluble graphene was acquired by dispersing 250 mg graphoil in 10 ml chlorosulphonic acid, centrifuging at 5,000 r.p.m. for 12 h, removing the top phase through a glass syringe, and quenching the top phase by slowly adding it to excess water. The quenching process produces solid graphene that could be entirely redispersed in chlorosulphonic acid with no insoluble portion. Using this source, soluble graphene was dispersed in chlorosulphonic acid at concentrations of 0.042 mg ml^{-1} (50 ppm by mass). Dispersions were prepared and mixed for 1 day in a glovebox (dew point −50 °C) in a nitrogen gas atmosphere to prevent contact with water and consequent evolution of gaseous hydrochloric acid. Samples (2 ml) of either dispersion were transferred into a vial and placed in the vitrification apparatus with a glass filter paper and glass pipette. The entire set-up was placed in a glove bag and purged with ultra-pure nitrogen (99.9995%) for 30 min. A drop of the graphene dispersion was then placed on 200 copper mesh, lacey carbon grid (Ted Pella). The glass filter paper (not reactive with chlorosulphonic acid) was then used to blot the sample, leaving a thin film of liquid. The grid was then quickly vitrified by dipping into liquid nitrogen (77 K) and was placed in a cryo-specimen holder for transfer into the TEM. Cryo-TEM imaging was carried out on an FEI T12 transmission electron microscope operated at 120 kV, using an Oxford CT3500 cooling holder, operated at about −180 °C.

XPS was performed on a PHI Quantera SXM scanning X-ray microprobe with a pass energy of 26.00 eV, 45° takeoff angle and a beam size of 100 μm.

Polarized light microscopy was performed on a Zeiss Axioplan microscope in transmission mode. The samples were sensitive to humidity and had to be sufficiently thin for light to be transmitted. Slide preparation was critical for preventing water contamination and for ensuring consistent sample thickness. Excessively thick samples appeared homogeneously dark simply due to the near-complete blockage of light. Glass slides and cover slips for microscopy were cleaned with diethyl ether and dried (100 °C, −25 mmHg, relative to atmospheric) overnight under vacuum and covered with aluminium foil. Slides were prepared in the glovebox, and the cover slips were sealed with aluminium tape. High-concentration samples were thinned by slowly hand-pressing on the cover slip to create a sufficiently thin region through which light was partially transmitted.

AFM images were obtained with a Digital Instruments Nanoscope IIIa, operating in tapping mode, using silicon tips n-doped with 1–10 Ω cm phosphorus (Veeco, MPP-11100-140) at a scan rate of 0.5 Hz and a resolution of 512 × 512.

AFM samples were prepared by transferring free-floating thin films on a silicon substrate.

Received 7 January 2010; accepted 6 April 2010; published online 30 May 2010

References

1. Segal, M. Selling graphene by the ton. *Nature Nanotech.* **4,** 612–614 (2009).
2. Novoselov, K. S. *et al.* Electric field effect transistor in atomically thin carbon film. *Science* **306,** 666–669 (2004).
3. Lee, C., Wei, X. D., Kysar, J. W. & Hone, J. Measurement of the elastic properties and intrinsic strength of monolayer graphene. *Science* **321,** 385–388 (2008).
4. Balandin, A. A. *et al.* Superior thermal conductivity of single-layer graphene. *Nano Lett.* **8,** 902–907 (2008).
5. Stankovich, S. *et al.* Graphene-based composite materials. *Nature* **442,** 282–286 (2006).
6. Schwamb, T., Burg, B. R., Schirmer, N. C. & Poulikakos, D. An electrical method for the measurement of the thermal and electrical conductivity of reduced graphene oxide nanostructures. *Nanotechnology* **20,** 405704 (2009).
7. Ruoff, R. Graphene: calling all chemists. *Nature Nanotech.* **3,** 10–11 (2008).
8. Novoselov, K. S. *et al.* Two-dimensional atomic crystals. *Proc. Natl Acad. Sci. USA* **102,** 10451–10453 (2005).
9. Hummers, W. S. & Offeman, R. E. Preparation of graphitic oxide. *J. Am. Chem. Soc.* **80,** 1339 (1958).
10. Stankovich, S. *et al.* Synthesis of graphene-based nanosheets via chemical reduction of exfoliated graphite oxide. *Carbon* **45,** 1558–1565 (2007).
11. Becerril, H. A. *et al.* Evaluation of solution-processed reduced graphene oxide films as transparent conductors. *ACS Nano* **2,** 463–470 (2008).
12. Hernandez, Y. *et al.* High-yield production of graphene by liquid-phase exfoliation of graphite. *Nature Nanotech.* **3,** 563–568 (2008).
13. Valles, C. *et al.* Solutions of negatively charged graphene sheets and ribbons. *J. Am. Chem. Soc.* **130,** 15802–15804 (2008).
14. Lotya, M. *et al.* Liquid phase production of graphene by exfoliation of graphite in surfactant/water solutions. *J. Am. Chem. Soc.* **131,** 3611–3620 (2009).
15. Davis, V. A. *et al.* True solutions of single-walled carbon nanotubes for assembly into macroscopic materials. *Nature Nanotech.* **4,** 830–834 (2009).
16. Cremlyn, R. J. *Chlorosulfonic Acid: A Versatile Reagent* (The Royal Society of Chemistry, 2002).
17. Melin, J., Furdin, G., Fuzellier, H., Vasse, R. & Herold, A. Action sur le graphite des solutions de chlorures dans l'acide chlorosulfonique. *Mater. Sci. Eng.* **31,** 61–65 (1977).
18. Rai, P. K. *et al.* Isotropic-nematic phase transition of single-walled carbon nanotubes in strong acids. *J. Am. Chem. Soc.* **128,** 591–595 (2006).
19. Ramesh, S. *et al.* Dissolution of pristine single walled carbon nanotubes in superacids by direct protonation. *J. Phys. Chem. B* **108,** 8794–8798 (2004).
20. Sumanasekera, G. U. *et al.* Electrochemical oxidation of single wall carbon nanotube bundles in sulfuric acid. *J. Phys. Chem. B* **103,** 4292–4297 (1999).
21. Cancado, L. G. *et al.* Measuring the degree of stacking order in graphite by Raman spetroscopy. *Carbon* **46,** 272–275 (2008).
22. Meyer, J. C. *et al.* On the roughness of single- and bi-layer graphene membranes. *Solid State Commun.* **143,** 101–109 (2007).
23. Onsager, L. The effects of shape on the interaction of colloidal particles *Ann. NY Acad. Sci.* **51,** 627–659 (1949).
24. Bates, M. A. & Frenkel, D. Nematic-isotropic transition in polydisperse systems of infinitely thin hard platelets. *J. Chem. Phys.* **110,** 6553–6559 (1999).
25. van der Kooij, F. M., Kassapidou, K. & Lekkerkerker, H. N. W. Liquid crystal phase transitions in suspensions of polydisperse plate-like particles. *Nature* **406,** 868–871 (2000).
26. Wensink, H. H. & Vroege, G. J. Isotropic-nematic phase behavior of length-polydisperse hard rods. *J. Chem. Phys.* **119,** 6868–6882 (2003).
27. Green, M. J., Parra-Vasquez, A. N. G., Behabtu, N. & Pasquali, M. Modeling the phase behavior of polydisperse rigid rods with attractive interactions with applications to single-walled carbon nanotubes in superacids. *J. Chem. Phys.* **131,** 084901 (2009).
28. van der Beek, D. & Lekkerkerker, H. N. W. Liquid crystal phases of charged colloidal platelets. *Langmuir* **20,** 8582–8586 (2004).
29. Chandrasekhar, S. *Liquid Crystals* 2nd edn (Cambridge Univ. Press, 1992).
30. Campos-Delgado, J. *et al.* Bulk production of a new form of *sp*(2) carbon: crystalline graphene nanoribbons. *Nano Lett.* **8,** 2773–2778 (2008).
31. Jiao, L. Y., Zhang, L., Wang, X. R., Diankov, G. & Dai, H. J. Narrow graphene nanoribbons from carbon nanotubes. *Nature* **458,** 877–880 (2009).
32. Kosynkin, D. V. *et al.* Longitudinal unzipping of carbon nanotubes to form graphene nanoribbons. *Nature* **458,** 872–875 (2009).
33. Talmon, Y. Transmission electron microscopy of complex fluids: the state of the art. *Ber. Bunsen Phys. Chem.* **100,** 364–372 (1996).

Acknowledgements

The authors acknowledge the helpful input of Y. Kauffmann, H. Schmidt, C. Young, M. Majumder, A. Mela, W. Adams and B. Chen. Funding was provided by Air Force Office of Scientific Research (AFOSR) grants FA9550-06-1-0207 and FA9550-09-1-0590, Department of Energy (DOE) (DE-FC-36-05GO15073), Air Force Research Laboratories (AFRL) agreements FA8650-07-2-5061 and 07-S568-0042-01-C1, the Robert A. Welch Foundation (C-1668), US Army Corps of Engineers Environmental Quality and Installation Program under grant W912HZ-08-C-0054, the USA–Israel Binational Science Foundation and the Evans–Attwell Welch Postdoctoral Fellowship. Mitsui & Co. generously donated the MWCNTs used for preparing the nanoribbons. Cryo-TEM was performed at the Electron Microscopy of Soft Matter Laboratory, supported by the Technion Russell Berrie Nanotechnology Institute (RBNI). The HRTEM work was

carried out at the Electron Microscopy Center at the Department of Materials Engineering, the Technion.

Author contributions

J.L. and N.B. conceived, designed and performed the experiments including dispersion and film fabrication. J.L. and A.S. performed AFM. N.B. and D.T. performed and interpreted the Raman measurements. N.B. characterized the liquid crystallinity. N.B. and A.N.G.P.V. designed the HRTEM experiments. A.S. fabricated the electronic devices. N.B., J.L. and A.S. performed electrical measurements. N.B. and A.S. performed SEM. N.B. performed STEM and electron diffraction. N.B. and A.L.H. prepared HRTEM samples, performed HRTEM experiments and interpreted the images. D.K. provided nanoribbons and graphite oxides. Y.T., Y.C., J.S., M.J.G. and E.K. performed HRTEM and cryo-TEM experiments and interpreted the images. N.B., M.J.G., A.L.H., A.S., J.L., Y.T., J.M.T. and M.P. co-wrote the paper. M.P., Y.T., Y.C. and J.M.T. supervised the project.

Additional information

The authors declare no competing financial interests. Supplementary information accompanies this paper at www.nature.com/naturenanotechnology. Reprints and permission information is available online at http://npg.nature.com/reprintsandpermissions/. Correspondence and requests for materials should be addressed to J.M.T. and M.P.